The Journal of Physical Chemistry A

 VOLUME 102, NUMBER 51, DECEMBER 17, 1998

FEATURE ARTICLE

Mixed Quantum/Classical Dynamics of Hydrogen Transfer Reactions

Sharon Hammes-Schiffer

Department of Chemistry and Biochemistry, University of Notre Dame, Notre Dame, Indiana 46556

Received: July 31, 1998; In Final Form: October 14, 1998

This article presents the methodology we have developed for the simulation of hydrogen transfer reactions, including multiple proton transfer and proton-coupled electron transfer reactions. The central method discussed is molecular dynamics with quantum transitions (MDQT), which is a mixed quantum/classical surface hopping method that incorporates nonadiabatic transitions between the proton vibrational and/or electronic states. The advantages of MDQT are that it accurately describes branching processes (i.e., processes involving multiple pathways), is valid in the adiabatic and nonadiabatic limits and the intermediate regime, and provides real-time dynamical information. The multiconfigurational MDQT (MC-MDQT) method combines MDQT with an MC-SCF formulation of the vibrational modes for the simulation of processes involving multiple quantum modes (e.g., for multiple proton transfer reactions). MC-MDQT incorporates the significant correlation between the quantum modes in a computationally practical way and has been applied to proton transport along water chains. The EV-MDQT method incorporates transitions between mixed electronic/proton vibrational adiabatic states, which are calculated in a way that removes the standard double adiabatic aproximation. EV-MDQT has been applied to model proton-coupled electron transfer reactions. These new developments allow the simulation of a wide range of biologically and chemically important hydrogen transfer processes.

I. Introduction

Hydrogen transfer reactions play a critical role in a variety of important chemical and biological processes. Often the hydrogen transfer reaction is coupled to other hydrogen transfer reactions or to an electron transfer reaction. For example, a wide range of enzymes, including serine proteases,[1,2] alcohol dehydrogenases,[3] and carbonic anhydrases,[4] involve proton relay systems, which are sequences of coupled proton transfer reactions. Moreover, the coupling between proton motion and electron transfer plays an important role in the conduction of electrons through proteins such as cytochrome *c*.[5,6] The vital processes of photosynthesis[7−9] and respiration[10−12] involve both multiple proton transfer and proton-coupled electron transfer (PCET) reactions. Our goal is to utilize computer simulation to help elucidate the underlying fundamental principles of these important processes.

The simulation of hydrogen transfer reactions requires a potential energy surface that incorporates quantum mechanical effects such as the formation and breaking of bonds and changes in charge distribution. Standard molecular mechanical (MM) potentials (i.e., standard parametrized analytical functional forms such as those presented in refs 13 and 14) do not incorporate these effects. These quantum mechanical effects can be incorporated into the potentials in several different ways. One approach is to include parametrized terms of suitable analytical forms that are fit to ab initio calculations.[15,16] A second approach is the Car−Parrinello method,[17] where a partial electronic structure calculation (typically based on density functional theory) of the entire system is performed at each molecular dynamics time step. A third approach is to combine quantum mechanical and molecular mechanical methods (the QM/MM methods), where reacting portions of the system are treated

10.1021/jp983246n CCC: $15.00
Published on Web 12/02/1998

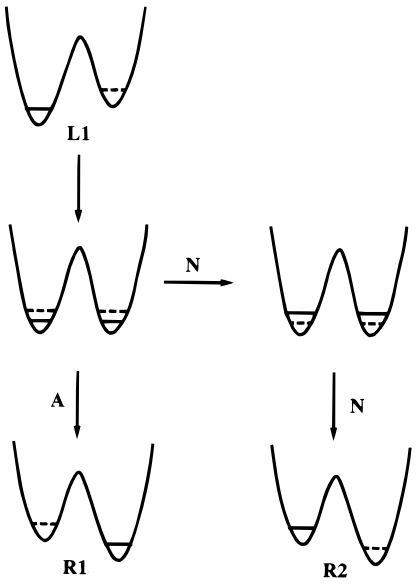

Figure 1. Schematic illustration of a branching process for a single proton transfer reaction. Each double well potential curve represents the potential in which the hydrogen atom moves for a particular classical configuration. The lowest two adiabatic proton quantum states are shown for each potential curve, and the occupied adiabatic state is indicated with a solid line. The potential curves are labeled using the following notation: L indicates that the left well is lower than the right well, and R indicates that the right well is lower than the left well. 1 indicates that the lowest energy adiabatic state is occupied, and 2 indicates that the second lowest energy adiabatic state is occupied. Thus L1 indicates that the left well is lower and the lowest energy adiabatic state is occupied. The pathways are labeled with an A for adiabatic and an N for nonadiabatic.

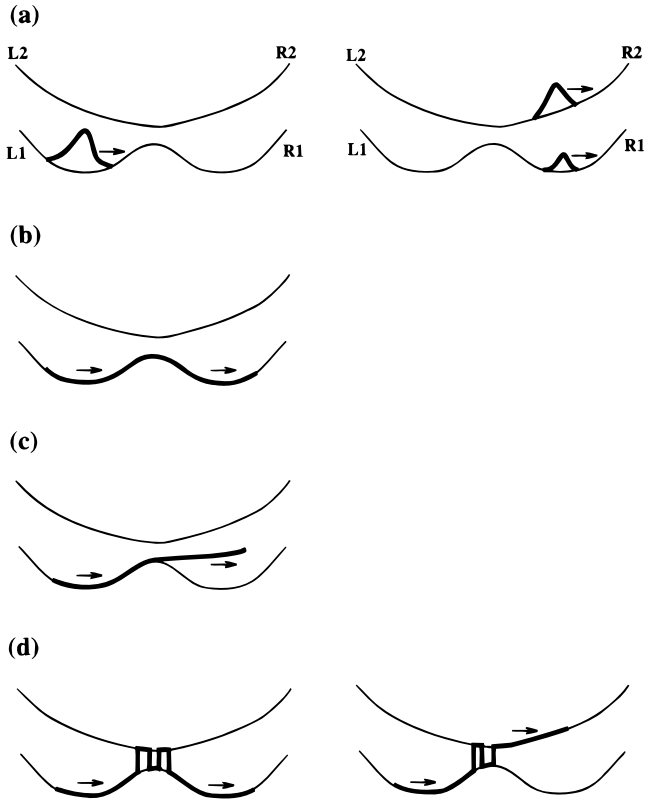

Figure 2. Schematic illustration of the two lowest energy adiabatic potential surfaces for a single proton transfer reaction as a function of the collective solvent mode, where the relevant configurations are labeled with the notation of Figure 1. (a) Schematic picture of a fully quantum mechanical wave packet calculation, where the solvent mode is represented initially as a single wave packet (shown on the left) that branches into two separate wave packets (shown on the right) when it passes through the region of strong nonadiabatic coupling. (b) Schematic picture of the trajectory resulting from an adiabatic calculation, where the trajectory remains on a single adiabatic surface. (c) Schematic picture of the trajectory resulting from a mean field calculation, where the trajectory follows an average path and ends up in a mixture of the two adiabatic states. (d) Schematic picture of two possible trajectories from an MDQT calculation, where each trajectory follows a single pathway and ends up on either the ground state (shown on the left) or the excited state (shown on the right) after passing through the region of strong nonadiabatic coupling.

quantum mechanically (using either ab initio or semiempirical electronic structure methods), while the remaining portions of the system are treated with standard MM potentials.[18−22] Thus, a broad spectrum of methods for obtaining potential energy surfaces for hydrogen transfer reactions is available.

Although the development of these types of potential energy surfaces is an important area of research, this article will focus on the *dynamical* aspects of hydrogen transfer reactions. Since the light mass of the transferring hydrogen atom(s) leads to quantum dynamical effects such as hydrogen tunneling, standard molecular dynamics simulations, in which all of the nuclei move classically, are inadequate for the simulation of hydrogen transfer reactions. Quantum dynamical effects such as hydrogen tunneling can be incorporated with mixed quantum/classical molecular dynamics methods, in which one or a few nuclei are treated quantum mechanically while the remaining nuclei are treated classically. For hydrogen transfer reactions typically the transferring hydrogen atom(s) are treated quantum mechanically, while the remaining atoms (i.e., the donor, acceptor, solvent, and/or protein) are treated classically. A number of mixed quantum/classical simulations have been developed and applied to proton transfer reactions in solution and in enzymes.[23−47] The various methods differ in the treatment of the interactions between the quantum and classical subsystems.

Figures 1 and 2 illustrate the fundamental dynamical issues involved in the simulation of hydrogen transfer reactions. Figure 1 depicts a schematic picture of a branching process for a single one-dimensional proton transfer reaction in solution. Each double well potential curve represents the potential in which the hydrogen atom moves for a particular solvent configuration. The shape of this double well potential changes as the solvent fluctuates, as indicated by the arrows. The lowest two adiabatic proton vibrational quantum states are shown for each curve, and the occupied adiabatic state is indicated with a solid line. If the system starts out in the ground state localized in the reactant well (configuration L1) and the solvent fluctuates so that the product well becomes lower in energy, then two possible pathways can be followed. The first is the adiabatic pathway, where the system remains in the ground state and the proton ends up localized in the product well (configuration R1). The second is the nonadiabatic pathway, where the system switches to the excited adiabatic state and thus the proton ends up localized in the reactant well (configuration R2). Figure 2 depicts the lowest two adiabatic potential energy surfaces as a function of a collective solvent mode for this branching process. These surfaces correspond to the energies of the two lowest adiabatic states for the double well potential curves shown in Figure 1 for different classical configurations. The branching process in Figure 1 corresponds to starting on the ground state in the L1 configuration, passing through the region of strong nonadiabatic coupling (the symmetric configuration), and following the adiabatic or the nonadiabatic pathway, ending up in either the

R1 or the R2 configuration, respectively. (Note that the nonadiabatic pathway requires a switch to the excited adiabatic potential energy surface.) Figure 2a illustrates a fully quantum mechanical calculation, where the solvent mode is represented initially as a single wave packet (shown on the left) that branches into two separate wave packets (shown on the right) when it passes through the region of strong nonadiabatic coupling. Note that the two separate wave packets move independently (i.e., are uncoupled) when they are far from the region of strong nonadiabatic coupling.

When the solvent mode is treated classically, the fundamental issue that arises is how the classical subsystem should evolve on these potential energy surfaces (i.e., the feedback from the quantum subsystem to the classical subsystem). In the standard adiabatic method,[27−29] the classical subsystem moves on a single adiabatic surface (typically the ground state) and thus always follows the adiabatic pathway, as shown in Figure 2b. This method is valid in the adiabatic limit (i.e., when the barrier is low) but will fail when there is a significant probability of following the nonadiabatic pathway. Similarly, perturbative methods have been developed for simulating proton transfer reactions in the nonadiabatic limit (i.e., when the barrier is high).[30] Since the barrier height for proton transfer depends on the distance between the donor and acceptor, which are typically vibrating, a single proton transfer reaction can span the adiabatic and nonadiabatic limits. Thus, although the adiabatic and nonadiabatic methods are extremely useful for certain systems, a more general method that can describe processes in both the adiabatic and nonadiabatic limits and the intermediate regime is desirable.

In the mean field methods,[47] the classical subsystem follows an average path derived from a mixture of adiabatic states (as shown in Figure 2c). These methods are useful in the adiabatic and nonadiabatic limits or when the adiabatic states exert similar forces on the classical subsystem. For many proton transfer reactions, however, the two states are of very different character (i.e., one ionic and one covalent) and thus exert different forces on the classical subsystem. In this case the mean field method does not generate the correct dynamics after passage through the region of strong nonadiabatic coupling if the classical subsystem moves according to a mixture of adiabatic states.[48]

The surface hopping methods[49−72] were designed to accurately describe these types of branching processes. In surface hopping, an ensemble of trajectories is propagated, and each trajectory moves classically on a single surface except for instantaneous transitions among the quantum states. Several different surface hopping algorithms have been developed, and these methods differ mainly in how the state switches are incorporated. In the molecular dynamics with quantum transitions (MDQT) surface hopping method,[23,63] these transitions are incorporated according to a probabilistic algorithm that ensures that the correct fraction of trajectories follows each pathway (as determined from the quantum probabilities derived from the time-dependent Schrödinger equation). Figure 2d illustrates two possible surface hopping trajectories, and an ensemble of such trajectories should resemble the wave packet dynamics shown in Figure 2a.

An alternative type of mixed quantum/classical molecular dynamics method is based on the Feynman path integral formalism.[37,38] Although path integral methods are extremely useful for calculating equilibrium properties, typically they employ a transition state theory approximation rather than directly predict real-time dynamical properties. Recently, however, much effort has been devoted to the development of path integral methods capable of calculating dynamical quantities.[73−77] One notable dynamical method of this type that has been applied to proton transfer reactions is the centroid molecular dynamics method.[45,74−77] Although these methods are very promising, they will not be discussed further here.

This article will describe the formulation of surface hopping for hydrogen transfer reactions and will present the methodology we have developed to address the additional challenges that arise for multiple proton transfer reactions and for proton-coupled electron transfer reactions. The first additional challenge that arises for these types of reactions is that the branching processes become more complicated, and the adiabatic potential surfaces involve many different regions of strong nonadiabatic coupling. The presence of multiple avoided curve crossings leads to quantum interference effects. We have shown that the phase-coherent surface hopping methods accurately describe these quantum interference effects.[78] The second additional challenge that arises is that the calculation of the adiabatic states becomes more difficult. For the case of multiple proton transfer reactions, the significant correlation between the transferring protons must be incorporated in a computationally practical manner. We have addressed this challenge by developing the multiconfigurational MDQT (MC-MDQT) method, which combines MDQT with a multiconfigurational self-consistent-field (MC-SCF) approach for vibrational modes.[79,80] For the case of proton-coupled electron transfer reactions, the adiabatic states are mixed electronic/proton vibrational states, and typically the standard double adiabatic approximation is not valid. To address this challenge, we developed the EV-MDQT method, which is based on a formulation for the calculation of mixed electronic/proton vibrational states that removes the standard double adiabatic approximation.[81]

An outline of this article is as follows. Section II describes the fundamental aspects of the application of surface hopping to hydrogen transfer reactions, including a method for simulating infrequent events for processes evolving on multiple potential energy surfaces. Section III presents the MC-MDQT method for mixed quantum/classical simulation of multiple quantum modes (e.g., multiple proton transfer reactions), and section IV presents the EV-MDQT method for processes involving nonadiabatic transitions among both proton vibrational and electronic states (e.g., proton-coupled electron transfer reactions). Concluding remarks are contained in section V.

II. Fundamental Aspects of Mixed Quantum/Classical Methods

Consider a general system consisting of N_c slow degrees of freedom (with masses M_I and coordinates $\mathbf{R}_I$) and N_q fast degrees of freedom (with masses m_i and coordinates $\mathbf{r}_i$). The total Hamiltonian is

$$H_{tot} = -\sum_{I=1}^{N_c} \frac{\hbar^2}{2M_I} \nabla_{\mathbf{R}_I}^2 + H_q(\mathbf{r},\mathbf{R}) \tag{1}$$

where

$$H_q(\mathbf{r},\mathbf{R}) = -\sum_{i=1}^{N_q} \frac{\hbar^2}{2m_i} \nabla_{\mathbf{r}_i}^2 + V(\mathbf{r},\mathbf{R}) \tag{2}$$

(Here $\mathbf{R}$ and $\mathbf{r}$ are vectors of dimension $3N_c$ and $3N_q$, respectively.) To separate the fast and slow coordinates, choose a set of L orthonormal basis functions $\{\Phi_n(\mathbf{r};\mathbf{R})\}$ for the fast coordinates $\mathbf{r}$. Note that these basis functions depend para-

metrically on the slow coordinates **R**. For simplicity in this article the basis functions $\Phi_n(\mathbf{r};\mathbf{R})$ are assumed to be real. The total wave function $\Psi(\mathbf{r},\mathbf{R},t)$ can be expanded in terms of these basis functions with time-dependent coefficients $\chi_n(\mathbf{R},t)$:

$$\Psi(\mathbf{r},\mathbf{R},t) = \sum_{n=1}^{L} \chi_n(\mathbf{R},t)\, \Phi_n(\mathbf{r};\mathbf{R}) \tag{3}$$

Substituting this into the time-dependent Schrödinger equation leads to the following set of coupled equations for the wave functions $\chi_n(\mathbf{R},t)$:

$$i\hbar \frac{\partial \tilde{\chi}(\mathbf{R},t)}{\partial t} = \tilde{H}\, \tilde{\chi}(\mathbf{R},t) \tag{4}$$

where $\tilde{\chi}$ is an L -dimensional vector with elements $\chi_n(\mathbf{R},t)$ and $\tilde{H}$ is an $L \times L$ matrix with elements

$$H_{ij}(\mathbf{R}) = K_{ij}(\mathbf{R}) + V_{ij}(\mathbf{R}) + D_{ij}(\mathbf{R}) + G_{ij}(\mathbf{R}) \tag{5}$$

$$K_{ij}(\mathbf{R}) = -\sum_{I=1}^{N_c} \frac{\hbar^2}{2M_I} \nabla^2_{\mathbf{R}_I} \delta_{ij} \tag{6}$$

$$V_{ij}(\mathbf{R}) = \langle \Phi_i | H_q(\mathbf{r},\mathbf{R}) | \Phi_j \rangle \tag{7}$$

$$D_{ij}(\mathbf{R}) = -\sum_{I=1}^{N_c} \frac{\hbar^2}{M_I} \langle \Phi_i | \nabla_{\mathbf{R}_I} \Phi_j \rangle \nabla_{\mathbf{R}_I} \tag{8}$$

and

$$G_{ij}(\mathbf{R}) = -\sum_{I=1}^{N_c} \frac{\hbar^2}{2M_I} \langle \Phi_i | \nabla^2_{\mathbf{R}_I} \Phi_j \rangle \tag{9}$$

Note that the brackets indicate integration over only the fast coordinates **r**. In the diabatic representation $D_{ij} = G_{ij} = 0$ for all i, j, so the propagation of eq 4 requires the calculation of only V_{ij}. In the adiabatic representation

$$H_q(\mathbf{r},\mathbf{R})\, \Phi_n(\mathbf{r};\mathbf{R}) = \epsilon_n(\mathbf{R})\, \Phi_n(\mathbf{r};\mathbf{R}) \tag{10}$$

so $V_{ij} = \epsilon_i \delta_{ij}$ and, in general, $D_{ij} \neq 0$ and $G_{ij} \neq 0$. Thus, in the adiabatic representation ϵ_i, D_{ij}, and G_{ij} must all be evaluated.

Often the diabatic representation is used for wave packet propagation on multiple surfaces.[82,83] For mixed quantum/classical simulations, however, the adiabatic representation is more convenient because the complete potential surfaces are not available, so the adiabatic basis functions $\Phi_n(\mathbf{r};\mathbf{R})$ and eigenenergies are obtained locally "on the fly" during the simulation. In other words, for each classical configuration sampled during the molecular dynamics simulation, the adiabatic basis functions and eigenenergies can be obtained by the numerical solution of the time-independent Schrödinger equation. As mentioned above, the adiabatic representation requires the calculation of D_{ij} and G_{ij} for the fully quantum wave packet calculations. Reference 84 shows that the calculation of both the D_{ij} and the G_{ij} terms does not involve the calculation of derivatives of the basis functions Φ_n but rather involves only the derivatives of the Hamiltonian H_q. Thus, these terms are straightforward to evaluate "on the fly". Note that eq 4 is exact for a complete basis set and can be propagated using standard numerical methods[85] for a small number of degrees of freedom.

For systems with more than a few slow degrees of freedom, however, the exact solution of eq 4 is computationally intractable. Thus mixed quantum/classical molecular dynamics methods, where the slow degrees of freedom **R** are treated classically and the fast degrees of freedom **r** are treated quantum mechanically, must be developed. In these methods the classical subsystem moves according to the standard equations of motion

$$M_I \ddot{\mathbf{R}}_I = \mathbf{F}^{\text{eff}}_{\mathbf{R}_I} = -\nabla_{\mathbf{R}_I} V^{\text{eff}}(\mathbf{R}) \tag{11}$$

where the effective potential $V^{\text{eff}}(\mathbf{R})$ differs for the various methods. The Hamiltonian $H_q(\mathbf{r},\mathbf{R}(t))$ becomes time-dependent through the classical trajectory $\mathbf{R}(t)$. The time-dependent wave function $\Psi(\mathbf{r},\mathbf{R},t)$ describing the quantum mechanical state at time t is expanded in terms of the instantaneous L orthonormal adiabatic basis functions $\Phi_j(\mathbf{r};\mathbf{R})$:

$$\Psi(\mathbf{r},\mathbf{R},t) = \sum_{j=1}^{L} C_j(t)\, \Phi_j(\mathbf{r};\mathbf{R}) \tag{12}$$

where $C_j(t)$ are complex-valued expansion coefficients (i.e., quantum amplitudes). Note that the adiabatic states $\Phi_j(\mathbf{r};\mathbf{R})$ are also time-dependent through the classical trajectory $\mathbf{R}(t)$. Substituting eq 12 into the time-dependent Schrödinger equation leads to

$$i\hbar \dot{C}_k = \sum_{j=1}^{L} C_j (V_{kj} - i\hbar \dot{\mathbf{R}} \cdot \mathbf{d}_{kj}) \tag{13}$$

where V_{kj} is defined in eq 7 and the nonadiabatic coupling vector $\boldsymbol{d}_{kj}(\mathbf{R})$ is defined as

$$\mathbf{d}_{kj}(\mathbf{R}) \equiv \langle \Phi_k | \nabla_{\mathbf{R}} \Phi_j \rangle = \frac{\langle \Phi_k | \nabla_{\mathbf{R}} H_q | \Phi_j \rangle}{\epsilon_j - \epsilon_k} \tag{14}$$

for $j \neq k$ and $\boldsymbol{d}_{kk} = 0$. Note that the nonadiabatic coupling vector $\boldsymbol{d}_{kj}(\mathbf{R})$ corresponds to the D_{ij} terms in eq 5, but the corresponding second derivative G_{ij} terms in eq 5 are rigorously absent in this formulation because the coefficients $C_j(t)$ depend only on time and not on the classical coordinates **R**. In density matrix notation the density matrix elements are defined as $a_{kj} \equiv C_k C_j^*$, where the diagonal density matrix elements a_{kk} are the occupation probabilities of the adiabatic states and the off-diagonal elements a_{kj} describe the coherence. In practice, eq 13 is integrated numerically, simultaneously with the integration of the classical trajectory $\mathbf{R}(t)$, to obtain the amplitudes $C_j(t)$ of each included quantum mechanical state.

As mentioned above, the various mixed quantum/classical methods differ in the definition of the effective potential $V^{\text{eff}}(\mathbf{R})$ for the classical subsystem. In the adiabatic methods,

$$V^{\text{eff}}(\mathbf{R}) = \epsilon_k(\mathbf{R}) = \langle \Phi_k | H_q | \Phi_k \rangle \tag{15}$$

where k is the occupied state, typically the ground state. In the mean field methods,

$$V^{\text{eff}}(\mathbf{R}) = \langle \Psi | H_q | \Psi \rangle \tag{16}$$

where Ψ is a mixture of adiabatic states given by eq 12. In the surface hopping methods each trajectory moves classically on a single adiabatic surface except for the possibility of instantaneous switches among the adiabatic states. Thus, the classical subsystem moves according to the effective potential given by eq 15, where the occupied state k is allowed to change. The "exact" forces corresponding to this potential are defined as

$$\mathbf{F}_{\mathbf{R}} = -\nabla_{\mathbf{R}} \langle \Phi_k | H_q | \Phi_k \rangle \tag{17}$$

For wave functions that are exact eigenfunctions of the Hamiltonian H_q, the Hellmann−Feynman theorem states that the force in eq 17 is identical to the Hellmann−Feynman force

$$\mathbf{F}_{\mathbf{R}}^{\mathrm{HF}} = -\langle \Phi_k | \nabla_{\mathbf{R}} H_q | \Phi_k \rangle \tag{18}$$

As discussed in ref 80, for an appropriate choice of basis functions the Hellmann−Feynman forces are rigorously identical to the exact forces even for approximate wave functions. Thus, typically the Hellmann−Feynman forces are used to numerically integrate the classical equations of motion.

This article centers on the molecular dynamics with quantum transitions (MDQT) surface hopping method.[23,63] The MDQT method implements Tully's fewest switches algorithm,[63] which correctly apportions trajectories among the states according to the quantum probabilities $|C_j(t)|^2$ (ignoring difficulties due to classically forbidden states) with the minimum required number of quantum transitions. In this algorithm the probability of switching states is defined in terms of the rate of change of the occupation probabilities, which can be derived from eq 13 to be

$$\dot{a}_{kk} = \sum_{j \neq k} b_{kj} \tag{19}$$

where

$$b_{jk} \equiv 2\hbar^{-1}\mathrm{Im}(a_{jk}^* V_{jk}) - 2Re(a_{jk}^* \dot{\mathbf{R}} \cdot \mathbf{d}_{jk}) \tag{20}$$

The rate of change of the occupation probability for state k due to coupling with state j is b_{kj}, so the change in the occupation probability for state k due to coupling with state j over a short time interval δt is $b_{kj}\delta t$. The number of state switches is minimized by assuming that the flux of probability between each pair of states results from probability transferring in only one direction. According to this algorithm, the probability of switching from the current state k to another state j during the time interval between t and $t + \delta t$ is

$$g_{kj}(t,\delta t) = \max\left(0, \frac{b_{jk}\delta t}{a_{kk}}\right) \tag{21}$$

where b_{jk} and a_{kk} are assumed to remain approximately constant during the short time interval δt and thus can be evaluated either at time t or at time $t + \delta t$. If $b_{jk} < 0$, then the occupation probability of the occupied state k can be viewed as increasing due to coupling with state j, so the probability of switching from state k to state j is zero. On the other hand, if $b_{jk} > 0$, then the occupation probability of the occupied state k can be viewed as decreasing due to coupling with state j, so the probability of switching from state k to state j is $b_{jk}\delta t/a_{kk}$. References 63 and 70 illustrate that this algorithm achieves the correct statistical populations of the states for model systems.

To determine whether a switch to any state j will occur, a uniform random number ξ ($0 < \xi < 1$) is selected at each time step in the trajectory. For example, if the occupied state $k = 1$, a switch to state 2 will occur if $\xi < g_{12}$, a switch to state 3 will occur if $g_{12} < \xi < g_{12} + g_{13}$, and so forth. If a switch to a different state j does occur and if $\epsilon_k \neq \epsilon_j$, then the velocities must be adjusted in order to conserve total energy. As described in ref 63, the velocities should be adjusted as if they were subjected to a force in the direction of the nonadiabatic coupling vector. If there is not enough velocity in the direction of the nonadiabatic coupling vector to maintain energy conservation, the system remains in the initial quantum state and the component of velocity in the direction of the nonadiabatic coupling vector is reversed.[23]

The fewest switches surface hopping algorithm possesses a number of advantageous properties. Since the transitions occur only when the occupation probabilities are changing rapidly in time, this algorithm ensures that the switching probabability vanishes in regions of vanishing nonadiabatic coupling, even if the time-dependent wave function is a mixture of adiabatic states. Thus, trajectories move adiabatically outside regions of strong nonadiabatic coupling, as required for the accurate description of branching processes. Furthermore, the regions of strong nonadiabatic coupling do not have to be identified in advance. Another important property is that the net switching probability during a finite length of time is independent of time step size: if the integration time step δt is reduced, then the switching probability per time step is reduced by the same factor while the number of steps in a finite length of time is increased by the same factor.

One of the critical issues in surface hopping methods is the treatment of the phase coherence. The standard MDQT method retains full coherence in the evolution of the quantum amplitudes (i.e., in the integration of eq 13). As discussed in ref 63, this coherent evolution of the quantum amplitudes is essential for the reproduction of quantum interference effects between successive regions of strong coupling. For condensed phase systems, however, quantum decoherence effects will be important. As discussed in refs 63 and 86, part of the quantum decoherence will be incorporated naturally in MDQT if a swarm of trajectories is propagated from the same classical initial conditions. Each trajectory will switch to a different state at a different time and thus will follow a different path. The divergence of these paths will lead to a loss of phase coherence for the swarm of trajectories. However, the accurate incorporation of decoherence in this manner could require a large ensemble of trajectories, which could be computationally prohibitive. In addition, the standard MDQT method does not include the part of the quantum decoherence associated with the quantum mechanical nature of the classical subsystem. Thus, various approaches have been devised to explicitly incorporate decoherence in MDQT or other related surface hopping methods. The simplest approach is to reset the quantum amplitudes according to a specified criterion such that the quantum amplitude is unity for the occupied state and is zero for all other states. One method of this type is to estimate a physically reasonable decoherence time and to reset the amplitudes at every decoherence time interval. This approach could be problematic if the amplitudes happened to be reset when the system is in the region of strong nonadiabatic coupling. In some cases the criterion for amplitude resetting is based on a physical characteristic of the specific system. For example, in the application of MDQT to proton transfer in solution presented in ref 23, the amplitudes were reset when the system reached the reactant or product region, as determined by the expectation value of the quantum proton coordinate. References 86 and 87 present a more sophisticated method for incorporating quantum decoherence effects into surface hopping simulations.

A number of other surface hopping methods have been developed.[49−72] Webster, Rossky, and Friesner have developed a surface hopping method (denoted the WRF method in this article) that utilizes the stationary phase semiclassical Pechukas force[88] to propagate the classical subsystem over each classical time step.[64,65] The WRF method implements a stochastic algorithm analogous to that used in MDQT to determine the occupied state. Since the WRF method uses mixed-state

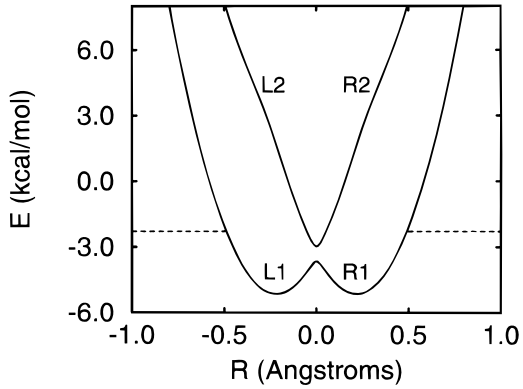

Figure 3. Adiabatic potential energy surfaces as a function of the collective solvent coordinate R for the model single proton transfer reaction. The surfaces are labeled according to the branching process depicted in Figure 1. The dashed lines indicate the flattening of the ground state at the boundaries to model solvent-induced stabilization.

propagation during each classical time step, it avoids the velocity rescaling required in the MDQT method during state switches. (Note that in the limit of infinitesimal time step, the MDQT velocity rescaling is identical to the WRF implementation of the Pechukas force.) Coker and co-workers[69] combined the long-time coherent integration of the quantum amplitudes of the MDQT method with the implementation of the Pechukas force of the WRF method. Unfortunately, the Pechukas force is nonlocal in time and thus requires a self-consistent iterative procedure that is significantly more computationally expensive than calculation of the adiabatic Hellmann−Feynman force used in the MDQT method. Recently Prezhdo and Rossky[71] presented a method that combines the fewest switches surface hopping algorithm of MDQT with a mean field force, which is of a similar computational cost as the adiabatic Hellmann−Feynman force. In this method the classical subsystem evolves on a mean field surface between state switches and is projected onto an adiabatic state when the mean field approximation becomes invalid. The investigation of semiclassical methods is also an active area of research.[89−91] Although these other methods are promising, the MDQT method is still appealing due to its conceptual and computational simplicity, as well as its high level of accuracy shown for a wide range of model systems.[63,78,84]

We have tested the accuracy of the MDQT method for describing hydrogen transfer reactions by comparing the MDQT and fully quantum mechanical methods for a simple model system of a single proton transfer reaction.[84] This model system includes one solvent degree of freedom representing a collective solvent mode and one hydrogen degree of freedom. The hydrogen moves in a double well potential, the solvent moves in a harmonic potential, and the two degrees of freedom are linearly coupled to each other. The lowest two adiabatic surfaces as a function of the solvent coordinate R are shown in Figure 3. Note that these surfaces closely resemble the schematic surfaces in Figure 2. The trajectories and the wavepackets were started in the L1 state and propagated until they reached one of the stable states L1 or R1. (Solvent-induced stabilization and decoherence effects were incorporated as described in ref 84.) As shown in Figure 2a, in the fully quantum mechanical calculation the initial wavepacket representing the solvent mode splits into two separate wavepackets, one on each surface, when it passes through the region of strong nonadiabatic coupling ($R = 0$ for this model system). In the MDQT calculations, an ensemble of trajectories corresponding to the initial wavepacket is propagated, and each trajectory moves classically on a single surface except for instantaneous transitions that typically occur

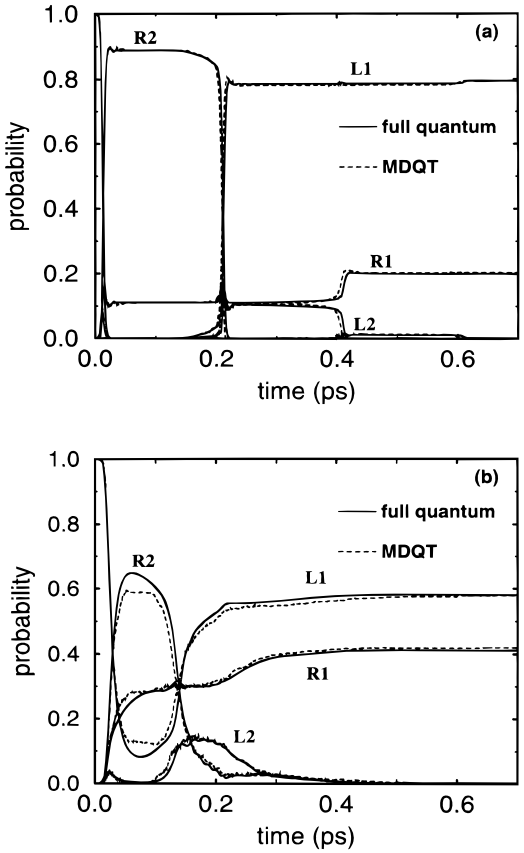

Figure 4. Time evolution of the populations of the adiabatic states shown in Figure 3 for the fully quantum (solid lines) and the MDQT (dashed lines) calculations for the model single proton transfer reaction. The curves are labeled according to Figure 3, and the initial conditions for the simulations are described in the text with (a) $P_o = 1200$ (amu Å)/ps and (b) $P_o = 600$ (amu Å)/ps.

in the region of strong nonadiabatic coupling (i.e., near $R = 0$ for this model system). Figure 2d schematically depicts two possible MDQT trajectories.

Figure 4 depicts the time evolution of the quantum probabilities for the quantum wave packet and the MDQT methods with two different initial wave packet momenta. The initial wave packet for the fully quantum calculation was on the ground state and of the form

$$\chi_1(R) = \left(\frac{2\alpha}{\pi}\right)^{1/4} e^{-\alpha(R-R_o)^2 + iP_o(R-R_o)/\hbar} \qquad (22)$$

where R_o, P_o, and α are parameters corresponding to the center, momentum, and width, respectively, of this wave packet. The corresponding initial conditions for the MDQT simulations were chosen according to the Wigner representation[92,93] of this initial wave packet. A swarm of 1000 trajectories was propagated for each initial quantum wave packet. The numerical methods for both the fully quantum mechanical and the MDQT calculations for this model system are described in ref 84. For $P_o = 1200$ (amu Å)/ps (shown in Figure 4a) the quantum wave packet and MDQT results are virtually indistinguishable. In this case the reaction is predominantly (90%) nonadiabatic. For $P_o = 600$ (amu Å)/ps (shown in Figure 4b) discrepancies in the probabilities of states R2 and L1 are evident between 0.05 and 0.1 ps, but the branching probabilities at 0.1 ps are in good agreement. Thus, Figure 4 illustrates that MDQT accurately calculates the branching probabilities for a wide range of initial momenta. We have also compared the MDQT and fully quantum

mechanical methods for analogous model systems including two solvent degrees of freedom and have shown that MDQT generates accurate branching probabilities for these types of systems.[48]

For the simple model described above, the exact quantum calculation is computationally faster than the MDQT calculation. For condensed phase systems with a large number of classical degrees of freedom, however, the exact quantum calculation is computationally impractical. Reference 23 presents the application of MDQT to a model developed by Azzouz and Borgis[42] for intramolecular proton transfer within a phenol−amine complex in liquid methyl chloride. In this model the phenol−amine complex was represented as a linear AH−B complex, and the classical solvent was represented by 255 rigid dipoles with periodic boundary conditions. The rates and kinetic isotope effects for this reaction are presented in ref 23. The results indicate that hydrogen tunneling and nonadiabatic effects are significant for this process. The effects of photoexcitation of the hydrogen motion for this model have also been investigated by initiating trajectories in an excited vibrational state localized in the reactant region.[36] This model serves as a stringent test of the MDQT method because it exhibits both adiabatic and nonadiabatic behavior. These simulations illustrate that MDQT is capable of treating both limits, as well as the intermediate regime. Moreover, these simulations demonstrate that the MDQT method is computationally practical for large condensed phase systems.

In this application of MDQT, the proton transfer reaction was fast enough that we were able to utilize direct simulation methods. Many interesting proton transfer reactions, however, involve a high energy barrier, rendering them too slow for direct simulation methods. In standard methods for simulating infrequent events (i.e., reactions that are slow due to a high energy barrier),[94−96] the total rate constant is expressed as the product of the classical transition state theory rate constant, which is the flux through a dividing surface (typically located in the bottleneck region), and a dynamical factor that accounts for recrossings of this dividing surface. The flux term can be calculated using standard statistical mechanical methods such as umbrella sampling. To calculate the dynamical correction factor, trajectories are started at the dividing surface and are integrated backward and forward in time. This calculation is problematic for simulations utilizing the MDQT method because it requires knowledge of the quantum amplitudes at the dividing surface, but the quantum amplitudes depend on the history of the trajectory. To address this problem, we developed a nonadiabatic transition state theory that serves as the basis of a new method for simulating infrequent events in reactions that evolve on multiple potential energy surfaces.[97] The fundamental principle of this infrequent events method is that an ensemble of trajectories is propagated (starting at the dividing surface) using an approximate surface hopping method that does not depend on the history of the trajectory, and then each trajectory is weighted in a way that reproduces the results for the true surface hopping method. This method has been applied in conjunction with MDQT to a one-dimensional two-state barrier crossing problem. The combination of MDQT and this method for simulating infrequent events allows the accurate simulation of a wide range of proton transfer reactions.

III. Treatment of Multiple Quantum Modes

In the initial applications of MDQT to proton transfer reactions only a single mode was treated quantum mechanically. Many processes, such as multiple proton transfer reactions, require the quantum mechanical treatment of multiple quantum modes. As discussed in section I, the extension of mixed quantum/classical methods to processes involving multiple quantum modes leads to several additional challenges.

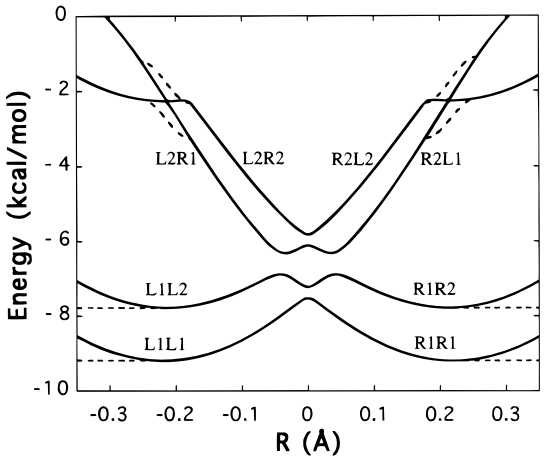

Figure 5. Adiabatic potential energy surfaces as a function of the collective solvent coordinate R for the model double proton transfer reaction. Only the four lowest energy adiabatic states are shown. To avoid numerical difficulties, the avoided crossing regions between the third and fourth states are smoothed out as shown by the dashed lines. The curves for the first two states are flattened, as shown by the dashed lines, to incorporate solvent-induced stabilization.

The first additional challenge is that the branching processes become more complicated, so a larger number of adiabatic states and avoided curve crossings are involved. The treatment of phase coherence is critical for situations involving multiple avoided curve crossings due to the presence of quantum interference effects. Since the standard MDQT method maintains the coherence of the quantum amplitudes, these quantum interference effects should be described accurately. To test the MDQT method for such processes, we have studied a model system for double proton transfer.[78] This model includes two proton degrees of freedom and one solvent degree of freedom R, which represents a collective solvent mode. The protons move in double well potentials, the solvent moves in a harmonic potential, the solvent is linearly coupled to one proton, and the two protons are linearly coupled to each other. Figure 5 presents the potential energy curves for the lowest four adiabatic states, and Figure 6 is a schematic picture of the branching process that occurs when the system starts in the ground state with $R < 0$ (configuration L1L1), passes through the region of strong nonadiabatic coupling ($R = 0$), and follows one of three possible pathways (R1R1, R1R2, or R2L1). Details of this model are given in ref 78. Analogous to the single proton transfer reactions, in a fully quantum mechanical calculation the initial wave packet representing the solvent mode splits into three separate wave packets, one on each of the three lowest surfaces, when it passes through the region of strong nonadiabatic coupling ($R = 0$ for this model system). In the MDQT simulations, the classical trajectories corresponding to the initial wave packet typically switch from one curve to another at the avoided curve crossings near $R = 0$.

Figure 7 depicts the time evolution of the populations on the first four states for both MDQT and fully quantum mechanical calculations. The initial wave packet for the fully quantum wave packet propagation was on the ground state and of the form given in eq 22 with $\alpha = 150$ au^{-2}, $R_o = -0.25$ au, and $P_o = 30$ au. For the MDQT calculations both protons were treated quantum mechanically, and the solvent mode was treated classically. A total of 1020 MDQT trajectories were propagated

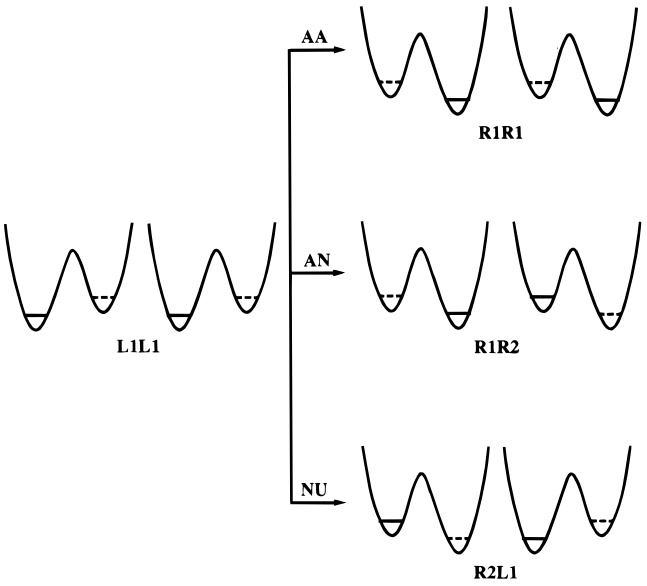

Figure 6. Schematic one-dimensional illustration of a branching process for a double proton transfer reaction. The notation is analogous to that in Figure 1, where R1R2 indicates that proton 1 is in configuration R1 and proton 2 is in configuration R2. The pathways are labeled with A for adiabatic, N for nonadiabatic, and U for unchanged, so AN indicates that proton 1 is adiabatic and proton 2 is nonadiabatic.

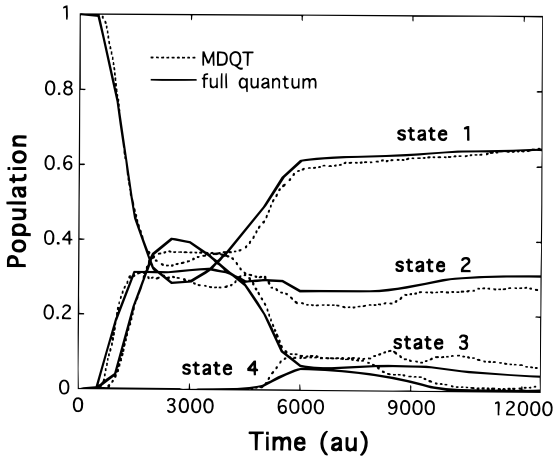

Figure 7. Time evolution of the populations of the adiabatic states shown in Figure 5 for fully quantum (solid lines) and MDQT (dashed lines) calculations for the model double proton transfer reaction.

with initial conditions chosen according to the Wigner representation of this initial wave packet. Numerical details are presented in ref 78. As for the single proton transfer model, the greatest discrepancies occur in the avoided crossing region, but the final branching probabilities are in good agreement. Thus, the MDQT method accurately treats the quantum interference effects for these types of processes.

The second challenge that arises for processes involving multiple quantum modes is that the calculation of the adiabatic states becomes more difficult since the significant correlation among the quantum modes must be incorporated in a computationally practical manner. To address this challenge, we have developed the multiconfigurational MDQT (MC-MDQT) method,[79,80] which combines an MC-SCF treatment of the vibrational modes with the MDQT method. In the MC-SCF formulation[98] for a general system of N quantum modes, the adiabatic eigenstates are approximated by a normalized linear combination of single configurations:

$$\Phi_n(\mathbf{r};\mathbf{R}) = \sum_J^Q d_{nJ}(\mathbf{R})\,\xi_J(\mathbf{r};\mathbf{R}) \tag{23}$$

where the single configurational wave functions $\xi_J(\mathbf{r};\mathbf{R})$ are products of the orthonormal one-particle states $\phi_{j_k}^{(k)}(r_k;\mathbf{R})$:

$$\xi_J(\mathbf{r};\mathbf{R}) = \prod_{k=1}^N \phi_{j_k}^{(k)}(r_k;\mathbf{R}) \tag{24}$$

Here $J = (j_1, j_2, ..., j_N)$ and Q is the total number of included configurations. Furthermore, each one-particle state $\phi_j^{(k)}(r_k;\mathbf{R})$ can be expanded in a basis of K_k fundamental one-particle basis functions $\chi_\alpha^{(k)}(r_k)$:

$$\phi_j^{(k)}(r_k;\mathbf{R}) = \sum_{\alpha=1}^{K_k} c_{j\alpha}^{(k)}(\mathbf{R})\,\chi_\alpha^{(k)}(r_k) \tag{25}$$

For simplicity each quantum particle is assumed to move in one dimension so that the coordinates r_k are scalar quantities, but the generalization to three-dimensional motion is conceptually straightforward. In addition, for simplicity this discussion is restricted to real basis functions, states, and configurations.

Application of the variational principle to the total energy $E = \langle\Phi_n|H_q|\Phi_n\rangle$ subject to the orthonormality conditions for the one particle wave functions $\phi_j^{(k)}$ and the adiabatic eigenstates Φ_n leads to a set of matrix equations for the configuration interaction coefficients d_{nJ} and the single particle expansion coefficients $c_{j\alpha}^{(k)}$. These matrix equations must be solved self-consistently for each classical configuration $\mathbf{R}$. Reference 80 presents an analytical proof that with an appropriate choice of basis functions the Hellmann−Feynman forces on the classical particles are equal to the "exact" forces (i.e., $\langle\Phi_n|\nabla_{\mathbf{R}}H_q|\Phi_n\rangle = \nabla_{\mathbf{R}}\langle\Phi_n|H_q|\Phi_n\rangle$) for these variational MC-SCF wave functions. Thus, the computationally expensive calculation of Pulay corrections[99] to the Hellmann−Feynman forces is avoided.

In the full configuration interaction method, the one particle states $\phi_{j_k}^{(k)}$ in eq 24 are equivalent to the fundamental one-particle basis functions $\chi_{j_k}^{(k)}$, so the configurations ξ are products of the fundamental basis functions. In this case the number of included configurations is $Q = \prod_{k=1}^N K_k$. This full configuration interaction method is computationally intractable for treating more than two or three modes quantum mechanically because the calculation of the adiabatic states (i.e., the solution of eq 10) becomes impractical for this large number of configurations.

The goal of the MC-SCF formulation is to choose physically reasonable single configurations so that the adiabatic states can be described with a significantly smaller number Q of single configurations than is required for the full configuration interaction method. One method for choosing physically reasonable configurations is the approximate MC-SCF method presented in ref 79, where the one-particle states are calculated using effective one-particle Hamiltonians derived from the occupied adiabatic state. In this method, the one-particle wave functions are calculated by solving the eigenvalue equation

$$h_{\text{eff}}^{(k)}\phi_j^{(k)}(r_k) = \epsilon_j^{(k)}\phi_j^{(k)}(r_k) \tag{26}$$

where

$$h_{\mathrm{eff}}^{(k)} = t_k + \sum_J^Q d_{nJ}^2 \left\langle \prod_{i\neq k}^N \phi_{j_i}^{(i)}(r_i) \middle| V(\mathbf{r},\mathbf{R}) \middle| \prod_{i\neq k}^N \phi_{j_i}^{(i)}(r_i) \right\rangle \quad (27)$$

Here t_k is the kinetic energy of quantum mode k, and n indicates the occupied multiconfigurational adiabatic state. The advantage of this approximate MC-SCF method is that it provides a clear physical picture of the reaction dynamics because each proton can be viewed as moving in a potential determined by both the occupied adiabatic state and the classical configuration. The one-particle adiabatic states can be calculated for each proton, and except for during branching processes each proton can be viewed as occupying a single one-particle adiabatic state. The multi-configurational mixing that occurs during branching processes is required to move from one single configurational adiabatic state to another. For example, the double well potential curves in Figure 6 represent single configurational adiabatic states, and the corresponding labels on the adiabatic states in Figure 5 indicate that far from the region of strong nonadiabatic coupling the adiabatic states are single configurational. The disadvantages of this approximate MC-SCF method are that it is not variational and that the Hellmann−Feynman forces are not rigorously equal to the "exact" forces.

Thus, the most accurate and robust method is to use the effective Hamiltonians from the approximate MC-SCF method to generate a physically reasonable starting guess for the wave function and, subsequently, to utilize the variational MC-SCF method to ensure accurate Hellmann−Feynman forces. Reference 80 compares this MC-SCF method to full configuration interaction calculations, and the remarkable agreement between the two methods for the forces and the ground and excited-state energies validates the use of this MC-SCF method for nonadiabatic molecular dynamics simulations. The MC-MDQT method combines this MC-SCF formulation with the MDQT method described above.

We have applied MC-MDQT to proton transport along chains of hydrogen-bonded water molecules, as shown in Figure 8.[100] This process is thought to play an important role in the fast translocation of protons over large distances in proteins. Recently, numerous simulations of proton transfer in water have been performed.[43−46,101−110] In our simulations the interactions in the protonated water chains were modeled by the PM6 dissociable polarization model developed by Stillinger and co-workers.[111−113] This potential is qualitatively but not quantitatively accurate. (In our current calculations we are using a multistate empirical valence bond model[110] to describe the interactions in the water chains.) Only those protons that form hydrogen bonds within the water chain were treated quantum mechanically. (The classical protons were constrained to a fixed O−H bond length in order to avoid nonphysical vibrational coupling between the quantum and classical protons.) The restricted number of quantum protons is due to the computational expense of the calculation of the many-body potential surface (and the associated forces) on a multidimensional grid. Thus, this is not an inherent limitation of the MC-SCF formulation or the MDQT method. The nonequilibrium starting conditions for these simulations were intended to mimic the situation in a transmembrane protein, where a proton is transferred from an amino acid to one end of a water chain that is embedded in a channel within the protein. Harmonic restraints on the oxygen atoms were utilized to mimic the structural restraints of the channel environment. In ref 100 the protons were induced to transfer along the chain by applying a linearly increasing external electric field. We have also studied the effects of hydrogen bonding and solvation by adding two solvating water molecules to each end of the chain.[114] Our nonequilibrium real-time quantum dynamical simulations of proton transport along water chains indicate that quantum dynamical effects such as hydrogen tunneling and nonadiabatic transitions are significant and that environmental effects such as fluctuating electric fields, structural constraints, hydrogen bonding, and solvation strongly impact this process. Future work will involve studying this process in a more realistic dynamical protein environment.

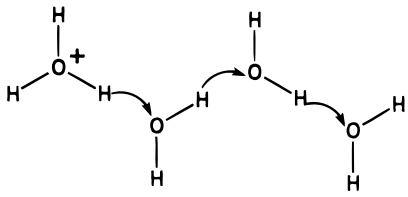

Figure 8. Schematic picture of proton transport along a protonated chain of four hydrogen-bonded water molecules.

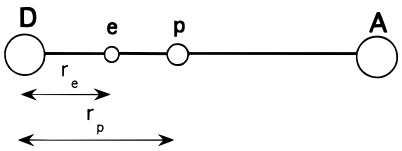

Figure 9. Schematic picture of the one-dimensional model system for PCET. D and A represent the electron donor and acceptor, and e and p represent the electron and proton. The proton donor and acceptor are not explicitly included in this plot but are implicitly assumed to lie along the axis between D and A. The details of this model are described in the text.

IV. Incorporation of Nonadiabatic Transitions between Both Electronic and Proton Vibrational States

Surface hopping methods were initially developed to incorporate transitions between electronic states[63−65] and later were extended to incorporate transitions between proton vibrational states.[23] (In addition, Herman and co-workers[61,62] have utilized surface hopping methods to study vibrational relaxation.) Some processes, such as proton-coupled electron transfer reactions, require the incorporation of transitions between both electronic and proton vibrational states. As discussed in section I, the extension of mixed quantum/classical methods to such processes leads to several additional challenges, including the accurate treatment of quantum interference effects due to a larger number of avoided curve crossings and the efficient calculation of mixed electronic/proton vibrational states.

To test the accuracy of MDQT for these types of systems and to study the fundamental principles of PCET, we developed a general PCET model that consists of three coupled degrees of freedom: an electron coordinate, a proton coordinate, and a solvent coordinate R.[115] This model system is illustrated in Figure 9. The electron donor and acceptor are fixed, and although not shown in this figure the proton donor and acceptor are also implicitly fixed on the $D-A$ axis. The solvent coordinate R, which is not shown in Figure 9, represents a collective solvent mode. The proton moves in a double well potential, and the solvent moves in a harmonic potential. The electron-donor, electron-acceptor, and electron-proton interactions are treated as modified Coulomb interactions, and the solvent mode is linearly coupled to the proton and the electron. Adjustment of the flexible parameters in this model generates a wide range of PCET mechanisms including concerted mechanisms (where the proton and electron are transferred simultaneously) and sequential mechanisms (where either the proton or the electron is

transferred first). In the MDQT calculations for these model systems the proton and electron coordinates were treated quantum mechanically, while the solvent coordinate was treated classically. Thus, the adiabatic quantum states were two-dimensional wave functions depending on both the electron and proton coordinates. We applied the MDQT method to a series of these model systems to study the fundamental principles of PCET.[115] In ref 115 the trajectories were initiated on the ground state, and in ref 116 the trajectories were initiated on the electronically excited state to simulate photoinduced PCET reactions. The MDQT simulations for this wide range of model PCET processes illustrated that nonadiabatic effects play an essential role in determining the rates and mechanisms of PCET reactions.

As mentioned above, one of the challenges for these types of processes is that the adiabatic potential surfaces involve multiple avoided curve crossings, so quantum interference effects are significant. To test the accuracy of MDQT for these types of processes we compared the MDQT method to fully quantum mechanical calculations for one of these model PCET systems.[78] Our results indicate that the MDQT method is accurate for these types of systems.

Another significant challenge that arises for these types of systems is the calculation of the mixed electronic/proton vibrational adiabatic states. The simplicity of the general model described above allowed us to calculate these adiabatic states using two-dimensional basis functions that were products of one-dimensional fundamental basis functions. In other words, the proton and electron were treated on equal footing. For more realistic systems involving many electrons, however, this approach is not computationally practical. For a general system with electronic degrees of freedom $\mathbf{r}_e$ (with mass m_e), quantum proton degrees of freedom $\mathbf{r}_p$ (with mass m_p), and N_s slow degrees of freedom $\mathbf{R}$ (with masses M_I), the total Hamiltonian is

$$H_{tot} = -\sum_{I=1}^{N_s} \frac{\hbar^2}{2M_I}\nabla^2_{\mathbf{R}_I} + H_f \tag{28}$$

where the Hamiltonian for the fast degrees of freedom (i.e., $\mathbf{r}_e$ and $\mathbf{r}_p$) is

$$H_f = -\frac{\hbar^2}{2m_e}\nabla^2_{\mathbf{r}_e} - \frac{\hbar^2}{2m_p}\nabla^2_{\mathbf{r}_p} + V(\mathbf{r}_e,\mathbf{r}_p,\mathbf{R}) \tag{29}$$

(Here $\nabla_{\mathbf{r}_e}{}^2$ and $\nabla_{\mathbf{r}_p}{}^2$ include sums over all electrons and quantum protons, respectively.) For a given classical configuration $\mathbf{R}$ the eigenfunctions $\Phi_k(\mathbf{r}_e,\mathbf{r}_p;\mathbf{R})$ of H_f are calculated by solving

$$H_f\Phi_k(\mathbf{r}_e,\mathbf{r}_p;\mathbf{R}) = E_k(\mathbf{R})\,\Phi_k(\mathbf{r}_e,\mathbf{r}_p;\mathbf{R}) \tag{30}$$

where

$$\Phi_k(\mathbf{r}_e,\mathbf{r}_p;\mathbf{R}) = \sum_\alpha c_{\alpha k}\xi_\alpha(\mathbf{r}_e,\mathbf{r}_p;\mathbf{R}) \tag{31}$$

Our goal is to choose the basis functions $\xi_\alpha(\mathbf{r}_e,\mathbf{r}_p;\mathbf{R})$ in a way that leads to the efficient calculation of the adiabatic states and provides a clear physical picture of the reaction dynamics. Our formulation is based on the double adiabatic approximation, where the electrons are assumed to respond instantaneously to the motion of the protons and the slow degrees of freedom, and the protons are assumed to respond instantaneously to the motion of the slow degrees of freedom. In this double adiabatic approximation, the electronic Hamiltonian is

$$H_e = -\frac{\hbar^2}{2m_e}\nabla^2_{\mathbf{r}_e} + V(\mathbf{r}_e,\mathbf{r}_p,\mathbf{R}) \tag{32}$$

and the electronic states for fixed ($\mathbf{r}_p$, $\mathbf{R}$) are obtained by solving

$$H_e\psi_i(\mathbf{r}_e;\mathbf{r}_p,\mathbf{R}) = \epsilon_i(\mathbf{r}_p,\mathbf{R})\,\psi_i(\mathbf{r}_e;\mathbf{r}_p,\mathbf{R}) \tag{33}$$

The proton vibrational Hamiltonian for electronic state i is

$$H_p^{(i)} = -\frac{\hbar^2}{2m_p}\nabla^2_{\mathbf{r}_p} + \epsilon_i(\mathbf{r}_p,\mathbf{R}) \tag{34}$$

and the proton vibrational states for fixed $\mathbf{R}$ and electronic state i are obtained by solving

$$H_p^{(i)}\phi_n^{(i)}(\mathbf{r}_p;\mathbf{R}) = \epsilon_n^{(i)}(\mathbf{R})\,\phi_n^{(i)}(\mathbf{r}_p;\mathbf{R}) \tag{35}$$

In the double adiabatic approximation, the eigenfunctions of H_f are approximated by

$$\xi_{in}(\mathbf{r}_e,\mathbf{r}_p;\mathbf{R}) = \psi_i(\mathbf{r}_e;\mathbf{r}_p,\mathbf{R})\phi_n^{(i)}(\mathbf{r}_p;\mathbf{R}) \tag{36}$$

with approximate eigenvalues $\epsilon_n^{(i)}(\mathbf{R})$. We have shown that the double adiabatic approximation is invalid for general proton-coupled electron transfer reactions.[81] Thus we remove the double adiabatic approximation by using the $\xi_{in}(\mathbf{r}_e,\mathbf{r}_p;\mathbf{R})$ in eq 36 as basis functions for the expansion given in eq 31. This definition of the basis functions provides a clear physical picture of the reaction dynamics because each adiabatic state can be viewed as predominately the product of an electronic and a proton vibrational state.

The matrix equation that must be solved to calculate the adiabatic states is of the form

$$\tilde{H}\tilde{c} = \tilde{c}\tilde{E} \tag{37}$$

and the matrix elements of the Hamiltonian $\tilde{H}$ are

$$\begin{aligned} H_{in,jm} &= \langle\xi_{in}|H_f|\xi_{jm}\rangle_{ep} \\ &= \delta_{ij}\delta_{mn}\epsilon_n^{(i)}(\mathbf{R}) - \frac{\hbar^2}{m_p}\langle\phi_n^{(i)}|\mathbf{d}_{ij}^{(ep)}\cdot\nabla_{\mathbf{r}_p}\phi_m^{(j)}\rangle_p - \\ &\qquad \frac{\hbar^2}{2m_p}\langle\phi_n^{(i)}|g_{ij}^{(ep)}\phi_m^{(j)}\rangle_p \end{aligned} \tag{38}$$

where

$$\mathbf{d}_{ij}^{(ep)}(\mathbf{r}_p,\mathbf{R}) = \langle\psi_i|\nabla_{\mathbf{r}_p}\psi_j\rangle_e = \frac{\langle\psi_i|\nabla_{\mathbf{r}_p}H_e|\psi_j\rangle_e}{\epsilon_j - \epsilon_i} \tag{39}$$

for $i \neq j$ and is zero for $i = j$, and

$$g_{ij}^{(ep)} = \langle\psi_i|\nabla^2_{\mathbf{r}_p}\psi_j\rangle_e \tag{40}$$

which can be expressed in terms of $\langle\psi_i|\nabla_{\mathbf{r}_p}H_e|\psi_j\rangle_e$ and $\langle\psi_i|\nabla^2_{\mathbf{r}_p}H_e|\psi_j\rangle_e$ using the expressions derived in ref 84. In these equations $\langle\,\rangle_{ep}$, $\langle\,\rangle_e$, and $\langle\,\rangle_p$ indicate integration over ($\mathbf{r}_e$, $\mathbf{r}_p$), $\mathbf{r}_e$, and $\mathbf{r}_p$, respectively. Moreover, $\tilde{c}$ has elements $c_{in,k}$, and $\tilde{E}$ is diagonal with elements E_k. Note that if $\mathbf{d}_{ij}^{(ep)} = g_{ij}^{(ep)} = 0$ then this formulation is identical to the double adiabatic approximation, where the ξ_{in} are the exact eigenfunctions of H_f with eigenvalues $\epsilon_n^{(i)}$.

The combination of this formulation with MDQT is denoted the EV-MDQT method (for electronic/vibrational adiabatic

states). In mixed quantum/classical simulations of these types of systems, the fast degrees of freedom ($\mathbf{r}_e$,$\mathbf{r}_p$) are treated quantum mechanically, while the slow degrees of freedom ($\mathbf{R}$) are treated classically. The MDQT methodology is the same as described above. In this case the nonadiabatic coupling vector can be evaluated as

$$\mathbf{d}_{kl}(\mathbf{R}) = \langle \Phi_k | \nabla_{\mathbf{R}} \Phi_l \rangle_{ep} = \frac{\sum_{in,jm} c_{in,k} c_{jm,l} \langle \phi_n^{(i)} | \mathbf{h}_{ij} \phi_m^{(j)} \rangle_p}{E_l - E_k} \quad (41)$$

for $k \neq l$ and $\boldsymbol{d}_{kk}(\mathbf{R}) = 0$. Here

$$\mathbf{h}_{ij}(\mathbf{r}_p,\mathbf{R}) = \langle \psi_i | \nabla_{\mathbf{R}} H_e | \psi_j \rangle_e \quad (42)$$

Note that in this formulation, the nonadiabatic coupling between the electron and proton is incorporated into the adiabatic states through eq 38, while the nonadiabatic couplings between the proton and solvent and between the electron and solvent appear in the nonadiabatic coupling vector $\boldsymbol{d}_{kl}(\mathbf{R})$ (given in eq 41). The calculation of all of these nonadiabatic coupling terms and the Hellmann−Feynman forces reduces to the calculation of the following three terms: $\langle \psi_i | \nabla_{\mathbf{r}_p} H_e | \psi_j \rangle_e$, $\langle \psi_i | \nabla^2_{\mathbf{r}_p} H_e | \psi_j \rangle_e$, and $\langle \psi_i | \nabla_{\mathbf{R}} H_e | \psi_j \rangle_e$ for fixed ($\boldsymbol{r}_p$,$\mathbf{R}$). Typically, these terms are straightforward to evaluate. We have applied the EV-MDQT formulation to the model PCET systems described above.[81]

The EV-MDQT methodology is applicable to a wide range of PCET reactions. Cukier and co-workers[117−120] have developed an extensive theory to predict the rate of a PCET reaction and have applied their methodology to experimentally studied model complexes consisting of electron donor−acceptor pairs juxtaposed by a hydrogen-bonding interface.[121−123] Currently, we are studying these types of model complexes with the EV-MDQT method in conjunction with a multistate empirical valence bond potential with explicit solvent.

V. Concluding Remarks

This article presents the methodology we have developed for the simulation of hydrogen transfer reactions, including multiple proton transfer and proton-coupled electron transfer reactions.[124] The MDQT surface hopping method has been applied to various hydrogen transfer reactions. The advantages of the MDQT method are that it describes branching processes accurately, is valid in the adiabatic and nonadiabatic limits and the intermediate regime, and provides real-time dynamical information. To simulate processes that are too slow for direct simulation methods, MDQT can be used in conjunction with a method for simulating infrequent events based on a nonadiabatic transition state theory.[97] Recently, the MC-MDQT method has been developed to simulate processes involving multiple quantum modes (e.g., multiple proton transfer reactions). MC-MDQT combines MDQT with an MC-SCF formulation for the vibrational modes in order to include the significant correlation between the quantum modes in a computationally practical way. In addition, recently the EV-MDQT method has been developed to simulate processes involving transitions between mixed electronic/proton vibrational adiabatic states (e.g., proton-coupled electron transfer reactions). EV-MDQT removes the standard double adiabatic aproximation and includes all nonadiabatic coupling terms in a computationally efficient way. All of these approaches provide a clear physical picture of the reaction dynamics. The combination of these new developments paves the way for the simulation of a wide range of hydrogen transfer processes.

Currently, we are applying this methodology to a broad spectrum of biologically and chemically important processes. For example, we are applying the MDQT method to proton and hydride transfer reactions in enzymes. We also plan to use the MC-MDQT method to study proton transport along water chains in transmembrane proteins such as bacteriorhodopsin. Moreover, we are utilizing the EV-MDQT method to investigate experimentally studied electron donor−acceptor pairs juxtaposed by a hydrogen-bonding interface.[121−123] In addition to these applications, we are continuing to investigate developments that will improve the accuracy and expand the applicability of this methodology.

The methodology described in this article represents only a very small part of a rapidly expanding field. We have not even attempted to present a complete overview of this field. The mixed quantum/classical simulation of hydrogen transfer reactions involves two main active areas of research. The first area is the development of more accurate potential energy surfaces to describe reactions in solution and in biological systems. Evidence of great progress in this area is illustrated by the broad range of available QM/MM potentials and the widespread use of the Car−Parrinello methodology[17] for calculating ab initio potential surfaces on the fly. The second area of research is the development of new approaches for incorporating nuclear quantum dynamical effects in condensed phase systems. In addition to the work discussed in this article, recent developments include path integral methods capable of calculating dynamical quantities[73−77] and a range of semiclassical approaches.[89−91,125,126] The combination of these two important areas of research represents the future of the field.

Acknowledgment. I would like to thank John Tully for introducing me to the field of mixed quantum/classical molecular dynamics. I would also like to thank members of my research group Hélène Decornez, Karen Drukker, Jian-Yun Fang, John Morelli, and Alexander Soudackov for their important contributions to the work discussed in this article. I am grateful for financial support from the NSF CAREER program grant CHE-9623813, the Petroleum Research Fund (administered by the ACS) grant No. 30432-G6, the Clare Boothe Luce Foundation, and an Alfred P. Sloan Foundation Research Fellowship.

References and Notes

(1) Blow, D. M. *Acc. Chem. Res.* **1976**, *9*, 145.
(2) Zundel, G. J. *Mol. Struct*. **1988**, *177*, 43.
(3) Sekhar, V. C.; Plapp, B. V. *Biochemistry* **1988**, *27*, 5082.
(4) Ren, X.; Tu, C.; Laipis, P. J.; Silverman, D. N. *Biochemistry* **1995**, *34*, 8492.
(5) Therien, M. J.; Selman, M.; Gray, H. B.; Chang, I.-J.; Winkler, J. R. *J. Am. Chem. Soc.* **1990**, *112*, 2420.
(6) Onuchic, J. N.; Beratan, D. N. *J. Chem. Phys.* **1990**, *92*, 722.
(7) Babcock, G. T.; Barry, B. A.; Debus, R. J.; Hoganson, C. W.; Atamian, M.; McIntosh, L.; Sithole, I.; Yocum, C. F. *Biochemistry* **1989**, *28*, 9557.
(8) Okamura, M. Y.; Feher, G. *Annu. Rev. Biochem.* **1992**, *61*, 861.
(9) Kirmaier, C.; Holten, D. *The Photosynthetic Bacterial Reaction Center—Structure and Dynamics*; Plenum: New York, 1988.
(10) Wikstrom, M. *Nature* **1989**, *338*, 776.
(11) Babcock, G. T.; Wikstrom, M. *Nature* **1992**, 356, 301.
(12) Malmstrom, B. G. *Acc. Chem. Res.* **1993**, *26*, 332.
(13) Brooks, B. R.; Bruccoleri, R. E.; Olafson, B. D.; States, D. J.; Swaminathan, S.; Karplus, M. *J. Comput. Chem*. **1983**, *4*, 187.
(14) Cornell, W. D.; Cieplak, P.; Bayly, C. I.; Gould, I. R.; K. M. Merz, J.; Ferguson, D. M.; Spellmeyer, D. C.; Fox, T.; Caldwell, J. W.; Kollman, P. A. *J. Am. Chem. Soc*. **1995**, *117*, 5179.
(15) Chandrasekhar, J.; Smith, S. F.; Jorgensen, W. L. *J. Am. Chem. Soc*. **1985**, *107*, 154.

(16) Scheiner, S.; Duan, X. Search for Analytical Functions to Simulate Proton Transfers in Hydrogen Bonds. In *Modeling the Hydrogen Bond*, Smith, D., Ed.; American Chemical Society: Washington, DC, 1994; Vol. 569, p 125.
(17) Car, R.; Parrinello, M. *Phys. Rev. Lett.* **1985**, *55*, 2471.
(18) Warshel, A.; Levitt, M. *J. Mol. Biol.* **1976**, *103*, 227.
(19) Singh, U.; Kollman, P. J. *Comput. Chem.* **1986**, *7*, 718.
(20) Field, M. J.; Bash, P. A.; Karplus, M. J. *Comput. Chem.* **1990**, *11*, 700.
(21) Aqvist, J.; Warshel, A. *Chem. Rev.* **1993**, *93*, 2523.
(22) Gao, J. *Acc. Chem. Res.* **1996**, *29*, 298.
(23) Hammes-Schiffer, S.; Tully, J. C. *J. Chem. Phys.* **1994**, *101*, 4657.
(24) Morillo, M.; Cukier, R. I. *J. Chem. Phys.* **1990**, *92*, 4833.
(25) Warshel, A.; Chu, Z. T. *J. Chem. Phys.* **1990**, *93*, 4003.
(26) Truhlar, D. G.; Liu, Y.-P.; Schenter, G. K.; Garrett, B. C. *J. Phys. Chem.* **1994**, *98*, 8396.
(27) Borgis, D.; Tarjus, G.; Azzouz, H. *J. Phys. Chem.* **1992**, *96*, 3188.
(28) Borgis, D.; Tarjus, G.; Azzouz, H. *J. Chem. Phys.* **1992**, *97*, 1390.
(29) Laria, D.; Ciccotti, G.; Ferrario, M.; Kapral, R. *J. Chem. Phys.* **1992**, *97*, 378.
(30) Borgis, D.; Hynes, J. T. *Chem. Phys.* **1993**, *170*, 315.
(31) Mavri, J.; Berendsen, H. J. C.; van Gunsteren, W. F. *J. Phys. Chem.* **1993**, *97*, 13469.
(32) Mavri, J.; Berendsen, H. J. C. *J. Phys. Chem.* **1995**, *99*, 12711.
(33) Staib, A.; Borgis, D.; Hynes, J. T. *J. Chem. Phys.* **1995**, *102*, 2487.
(34) Ando, K.; Hynes, J. T. *J. Mol. Liq.* **1995**, *64*, 25.
(35) Bala, P.; Lesyng, B.; McCammon, J. A. *Chem. Phys.* **1994**, *180*, 271.
(36) Hammes-Schiffer, S.; Tully, J. C. *J. Phys. Chem.* **1995**, *99*, 5793.
(37) Li, D.; Voth, G. A. *J. Phys. Chem.* **1991**, *95*, 10425.
(38) Hwang, J.-K.; Warshel, A. *J. Phys. Chem.* **1993**, *97*, 10053.
(39) Hwang, J.-K.; Chu, Z. T.; Yadav, A.; Warshel, A. *J. Phys. Chem.* **1991**, *95*, 8445.
(40) Lobaugh, J.; Voth, G. A. *Chem. Phys. Lett.* **1992**, *198*, 311.
(41) Lobaugh, J.; Voth, G. A. *J. Chem. Phys.* **1994**, *100*, 3039.
(42) Azzouz, H.; Borgis, D. *J. Chem. Phys.* **1993**, *98*, 7361.
(43) Pomès, R.; Roux, B. *Chem. Phys. Lett.* **1995**, *234*, 416.
(44) Pomès, R.; Roux, B. *J. Phys. Chem.* **1996**, *100*, 2519.
(45) Lobaugh, J.; Voth, G. A. *J. Chem. Phys.* **1996**, *104*, 2056.
(46) Billeter, S. R.; van Gunsteren, W. F. *Comput. Phys. Commun.* **1997**, *107*, 61.
(47) Bala, P.; Grochowski, P.; Lesyng, B.; McCammon, J. A. *J. Phys. Chem.* **1996**, *100*, 2535.
(48) Fang, J.-Y.; Hammes-Schiffer, S. To be submitted.
(49) Tully, J. C.; Preston, R. K. *J. Chem. Phys.* **1971**, *55*, 562.
(50) Miller, W. H.; George, T. F. *J. Chem. Phys.* **1972**, *56*, 5637.
(51) Stine, J. R.; Muckerman, J. T. *J. Chem. Phys.* **1976**, *65*, 3975.
(52) Blais, N. C.; Truhlar, D. G. *J. Chem. Phys.* **1983**, *79*, 1334.
(53) Blais, N. C.; Truhlar, D. G.; Mead, C. A. *J. Chem. Phys.* **1988**, *89*, 6204.
(54) Dunne, L. J.; Murrell, J. N.; Stamper, J. G. *Chem. Phys. Lett.* **1984**, *112*, 497.
(55) Parlant, G.; Gislason, E. A. *J. Chem. Phys.* **1989**, *91*, 4416.
(56) Parlant, G.; Alexander, M. H. *J. Chem. Phys.* **1990**, *92*, 2287.
(57) Kuntz, P. J. *J. Chem. Phys.* **1991**, *95*, 141.
(58) Kuntz, P. J.; Hogreve, J. J. *J. Chem. Phys.* **1991**, *95*, 156.
(59) Herman, M. F. *J. Chem. Phys.* **1984**, *81*, 754.
(60) Herman, M. F. *J. Chem. Phys.* **1984**, *81*, 764.
(61) Herman, M. F.; Arce, J. C. *Chem. Phys.* **1994**, *183*, 335.
(62) Arce, J. C.; Herman, M. F. *J. Chem. Phys.* **1994**, *101*, 7520.
(63) Tully, J. C. *J. Chem. Phys.* **1990**, *93*, 1061.
(64) Webster, F. J.; Schnitker, J.; Friedrichs, M. S.; Friesner, R.; Rossky, P. *Phys. Rev. Lett.* **1991**, *66*, 3172.
(65) Webster, F.; Rossky, P. J.; Friesner, R. A. *Comput. Phys. Commun.* **1991**, *63*, 494.
(66) Webster, F.; Wang, E. T.; Rossky, P. J.; Friesner, R. A. *J. Chem. Phys.* **1994**, *100*, 4835.
(67) Space, B.; Coker, D. F. *J. Chem. Phys.* **1991**, *94*.
(68) Space, B.; Coker, D. F. *J. Chem. Phys.* **1992**, *96*, 652.
(69) Coker, D. F.; Xiao, L. *J. Chem. Phys.* **1995**, *102*, 496.
(70) Coker, D. F. *Computer Simulation in Chemical Physics*; Kluwer Academic: Dordrecht, The Netherlands, 1993.
(71) Prezhdo, O. V.; Rossky, P. J. *J. Chem. Phys.* **1997**, *107*, 825.
(72) Topaler, M. S.; Allison, T. C.; Schwenke, D. W.; Truhlar, D. G. *J. Phys. Chem. A* **1998**, *102*, 1666.
(73) Makri, N. *Comput. Phys. Comm.* **1991**, *63*, 389.
(74) Cao, J.; Voth, G. A. *J. Chem. Phys.* **1993**, *99*, 10070.
(75) Cao, J.; Voth, G. A. *J. Chem. Phys.* **1994**, *100*, 5106.
(76) Cao, J.; Voth, G. A. *J. Chem. Phys.* **1994**, *101*, 6157.
(77) Cao, J.; Voth, G. A. *J. Chem. Phys.* **1994**, *101*, 6168.
(78) Fang, J.-Y.; Hammes-Schiffer, S. *J. Chem. Phys.* **1997**, *107*, 8933.
(79) Hammes-Schiffer, S. *J. Chem. Phys.* **1996**, *105*, 2236.
(80) Drukker, K.; Hammes-Schiffer, S. *J. Chem. Phys.* **1997**, *107*, 363.
(81) Soudackov, A. V.; Hammes-Schiffer, S. *Chem. Phys. Lett.*, in press.
(82) Kotler, Z.; Nitzan, A.; Kosloff, R. *Chem. Phys. Lett.* **1988**, *153*, 483.
(83) Campos-Martinez, J.; Waldeck, J. R.; Coalson, R. D. *J. Chem. Phys.* **1992**, *96*, 3613.
(84) Morelli, J.; Hammes-Schiffer, S. *Chem. Phys. Lett.* **1997**, *269*, 161.
(85) Tal-Ezer, H.; Kosloff, R. *J. Chem. Phys.* **1984**, *81*, 3967.
(86) Schwartz, B. J.; Bittner, E. R.; Prezhdo, O. V.; Rossky, P. J. *J. Chem. Phys.* **1996**, *104*, 5942.
(87) Bittner, E. R.; Rossky, P. J. *J. Chem. Phys.* **1995**, *103*, 8130.
(88) Pechukas, P. *Phys. Rev.* **1969**, *181*, 174.
(89) Neria, E.; Nitzan, A. *J. Chem. Phys.* **1993**, *99*, 1109.
(90) Jungwirth, P.; Gerber, R. B. *J. Chem. Phys.* **1996**, *104*, 5803.
(91) Martinez, T. J.; Ben-Nun, M.; Levine, R. D. *J. Phys. Chem.* **1996**, *100*, 0, 7884.
(92) Wigner, E. *Phys. Rev.* **1932**, *40*, 749.
(93) Heller, E. J. *J. Chem. Phys.* **1976**, *65*, 1289.
(94) Keck, J. C. *J. Chem. Phys.* **1960**, *32*, 1035.
(95) Anderson, J. B. *J. Chem. Phys.* **1973**, *58*, 4684.
(96) Bennett, C. H. *Algorithms for Chemical Computation*; American Chemical Society: Washington, DC, 1997.
(97) Hammes-Schiffer, S.; Tully, J. C. *J. Chem. Phys.* **1995**, *103*, 8528.
(98) Tobin, F. L.; Bowman, J. M. *Chem. Phys.* **1980**, *47*, 151.
(99) Pulay, P. *Applications of Electronic Structure Theory*; Modern Theoretical Chemistry; Plenum Press: New York, 1977; Vol. 4.
(100) Drukker, K.; de Leeuw, S.; Hammes-Schiffer, S. *J. Chem. Phys.* **1998**, *108*, 6799.
(101) Duan, X.; Scheiner, S. *J. Mol. Struct.* **1992**, *270*, 173.
(102) Cheng, H.-P.; Barnett, R. N.; Landman, U. *Chem. Phys. Lett.* **1995**, *237*, 161.
(103) Tuckerman, M.; Laasonen, K.; Sprik, M.; Parrinello, M. *J. Chem. Phys.* **1995**, *103*, 150.
(104) Tuckerman, M. E.; Marx, D.; Klein, M. L.; Parrinello, M. *Science* **1997**, *275*, 817.
(105) Kreuer, K.-D. *Chem. Mater.* **1996**, *8*, 610.
(106) Schmidt, R. G.; Brickmann, J. *Ber. Bunsen-Ges. Phys. Chem.* **1997**, *101*, 1816.
(107) Agmon, N. *Chem. Phys. Lett.* **1995**, *244*, 456.
(108) Vuilleumier, R.; Borgis, D. *Chem. Phys. Lett.* **1998**, *284*, 71.
(109) Vuilleumier, R.; Borgis, D. *J. Phys. Chem. B* **1998**, *102*, 4261.
(110) Schmitt, U.; Voth, G. A. *J. Phys. Chem. B* **1998**, *102*, 5547.
(111) Stillinger, F. H.; David, C. W. *J. Chem. Phys.* **1978**, *69*, 1473.
(112) Weber, T. A.; Stillinger, F. H. *J. Phys. Chem.* **1982**, *86*, 1314.
(113) Stillinger, F. H. *J. Chem. Phys.* **1979**, *71*, 1647.
(114) Decornez, H.; Drukker, K. D.; Hammes-Schiffer, S. To be submitted.
(115) Fang, J.-Y.; Hammes-Schiffer, S. *J. Chem. Phys.* **1997**, *106*, 8442.
(116) Fang, J.-Y.; Hammes-Schiffer, S. *J. Chem. Phys.* **1997**, *107*, 5727.
(117) Cukier, R. I. *J. Phys. Chem.* **1994**, *98*, 2377.
(118) Zhao, X. G.; Cukier, R. I. *J. Phys. Chem.* **1995**, *99*, 945.
(119) Cukier, R. I. *J. Phys. Chem.* **1995**, *99*, 16101.
(120) Cukier, R. I. *J. Phys. Chem.* **1996**, *100*, 15428.
(121) Turro, C.; Chang, C. K.; Leroi, G. E.; Cukier, R. I.; Nocera, D. G. *J. Am. Chem. Soc.* **1992**, *114*, 4013.
(122) Roberts, J. A.; Kirby, J. P.; Nocera, D. G. *J. Am. Chem. Soc.* **1995**, *117*, 8051.
(123) Kirby, J. P.; Roberts, J. A.; Nocera, D. G. *J. Am. Chem. Soc.* **1997**, *119*, 9230.
(124) Hammes-Schiffer, S. *Advances in Classical Trajectory Methods*; JAI Press Inc.: London, 1998; Vol. 3, pp 73−119.
(125) Herman, M. F. *J. Chem. Phys.* **1995**, *103*, 8081.
(126) Sun, X.; Miller, W. H. *J. Chem. Phys.* **1997**, *106*, 6346.